Renewable Energy 193 (2022) 832–842

Contents lists available at ScienceDirect

Renewable Energy

journal homepage: www.elsevier.com/locate/renene

Power improvement of a cluster of three Savonius wind turbines using the variable-speed control method

Yunrui Chen , Penghua Guo , Dayu Zhang , Kaixin Chai , Chenxi Zhao , Jingyin Li *

School of Energy and Power Engineering, Xi'an Jiaotong University, Xi'an, 710049, Shaanxi, China

ARTICLE INFO

Article history:
Received 23 December 2021
Received in revised form
9 May 2022
Accepted 10 May 2022
Available online 18 May 2022

Keywords:
Savonius wind turbine
Coupling effect
Variable-speed control method

ABSTRACT

The average power output of multiple Savonius wind turbines optimally arranged in a cluster is improved significantly compared to that of an isolated turbine due to the coupling effect. Previous investigations focused on the influence of the configuration and the initial phase angles of Savonius turbines operating at the same rotational speed in a cluster. This paper proposes to adopt the variable-speed control method to improve the power output of a three-turbine cluster, and simultaneously avoid the requirement for the accurate initial phase angle settings of the turbines. The Taguchi method is used to optimize the configuration of the cluster. The distances between the centers of adjacent turbines ($L_{1\text{-}2}$, $L_{1\text{-}3}$), the configuration angles ($\theta_{1\text{-}2}$, $\theta_{1\text{-}3}$), and the combination of rotational directions (RD) are taken as Taguchi experimental factors. The optimal configuration of the cluster is determined to be $L_{1\text{-}2} = 2.0D$, $L_{1\text{-}3} = 2.4D$, $\theta_{1\text{-}2} = 110°$, $\theta_{1\text{-}3} = 110°$, and RD = (-,+,-). The influence strength of the factors is ranked as configuration angle, RD, and distance between turbines. In addition, the average power coefficient of the turbines in the optimal cluster is 1.425 times that of an isolated turbine and the tip speed ratios of the three turbines are 1.13, 1.14, and 1.09.

© 2022 Elsevier Ltd. All rights reserved.

1. Introduction

As a type of vertical axis wind turbine (VAWT), the Savonius wind turbine has attracted much attention in recent years because of its simple structure, good self-starting performance and suitability for small-scale power generation [1]. Many types of research focused on the blade profile [2,3], blade number [4,5], overlap ratio [6], aspect ratio [7], twisted blade [8,9], endplates [10], and stage number [11,12], of an isolated Savonius wind turbine, to improve its power coefficient (C_P). The effects of deflectors [13,14] and Savonius-Darrieus type turbine [15] on the performance of the conventional Savonius turbine have also been studied. Recent investigations showed that Savonius turbines arranged reasonably in a cluster or a farm can obtain a much higher power coefficient than that of an isolated turbine due to the coupling enhancement effect [16]. This is a special feature for Savonius turbine arrays, compared with the widely used horizontal axis wind turbines.

A few experimental investigations have been conducted to study the interaction effect between two Savonius turbines. For example, the early study of Ogawa [17] measured the variations in the total power output of two Savonius wind turbines by changing the separation distance, phase angle, and rotational direction. Results showed that the average power output per turbine was 1.12 times that of an isolated turbine when the three parameters were set at a suitable value. Golecha et al. [18] tested the performance of two hydrokinetic Savonius turbines arranged in tandem, investigating the influence of the distance between the two turbines. This work indicated that the performance of one turbine is affected by the other when the distance is within 8 times the radius of the upstream turbine. On the other hand, Jang et al. [19] placed two Savonius turbines side by side which was perpendicular to the incoming flow, to investigate the influence of the rotational direction and distance between the turbines on power output. The results showed a 15% improvement in the average power coefficient ($\overline{C_P}$) was achieved at a specific installation of two turbines. Shigetomi et al. [20] used particle image velocimetry to investigate the flow field around an array of two Savonius wind turbines. They indicated that the interaction mechanisms between the two turbines are the Magnus effect and the periodic coupling of local flow. Nag and Sarkar [21] experimentally studied the performance of two Helical Savonius hydrokinetic turbines (HSHKTs), which are placed similarly to Ref. [18]. An optimal distance of 4 times of diameter ($4D$) between two turbines and made a comparison with CFD results is presented.

Computational Fluid Dynamic (CFD) is a powerful tool to

* Corresponding author.
E-mail address: jyli@mail.xjtu.edu.cn (J. Li).

https://doi.org/10.1016/j.renene.2022.05.062
0960-1481/© 2022 Elsevier Ltd. All rights reserved.

conduct detailed investigations of flow fields. Therefore, many researchers investigated the interaction effect and the complex unsteady flow fields caused by the coupling effect among multiple Savonius turbines by CFD methods. In addition, the three-turbine cluster is the basic unit configuration for different arrays, so the three-turbine cluster is often taken as a basis to study the coupling effect and configuration design for an array of Savonius turbines. For example, Shaheen et al. [22] used two-dimensional (2-D) simulations to optimize the power output of a cluster of three co-rotating Savonius turbines arranged in an isosceles triangle configuration, in which the three turbines have a common tip speed ratio (*TSR*) of 1. The simulated $\overline{C_P}$ was improved by 34% compared with their corresponding isolated turbine. In the following study, Shaheen and Abdallah [23] placed this efficient three-turbine cluster in wind turbine farms for two cases which included 9 and 27 turbines in total, and the power output reached 1.26 times and 1.37 times that of an isolated turbine. Zheng et al. [24] used 2-D simulations and Genetic Algorithm to optimize the configuration of a three-turbine cluster with the fixed rotational direction of the center turbine. An up to 37% increase in $\overline{C_P}$ was obtained for the optimal cluster at a *TSR* of 0.8. El-Baz et al. [25] investigated the performance of a three Savonius turbine cluster located in a specific isosceles triangle with the same initial phase angle and speed, but the rotational directions of turbines are different. An increase of up to 44% in $\overline{C_P}$ was obtained, compared with that of an isolated turbine, and the evident performance improvement was attributed to the high-speed flow accelerated by the favorable interaction between turbines. Nag and Sarkar [21] simulated three HSHKTs in triangular and staggered formations and found better performance in staggered formation than that in triangular formation. Other configurations of a three-turbines cluster [26] or more turbines in line arrays [16,27,28] were also investigated.

In the studies mentioned above, the turbines in a cluster or array all operate at the same rotational speed. For the constant-speed Savonius turbine cluster or array, the initial phase angles of the turbines play an important role in power enhancement and interaction, especially in close proximity. Sun et al. [29] have studied the effect of initial phase angle and distance between turbines on the performance of two-turbine and three-turbine clusters with the same rotational speed. They reported that the $\overline{C_P}$ of a side by side two-turbine cluster with a difference of 90° of the initial phase angle was approximately as high as twice that with an initial phase difference of 0°. For an isosceles triangle cluster of three turbines, the difference in $\overline{C_P}$ could be up to 50% due to different combinations of the initial phase angles. Therefore, the initial phase angle should be taken into consideration both in the optimization of the configuration of turbine arrays and in practice. However, an accurate setting of the initial phase angles for all the turbines in arrays or farms is difficult.

In this paper, the variable-speed control method is proposed to make the Savonius turbines operate at their optimal power points. Hence, the *TSR* and the initial phase angle do not need to be taken into consideration in the optimization, which reduces the optimization variables evidently. In addition, the strict demand for initial phase angles can also be avoided in practice. The Taguchi method is used to optimize the configuration and rotational direction of a cluster of three turbines by using the variable-speed control method.

2. Numerical method and validation

2.1. Turbine geometry and computational domain

A Savonius wind turbine model with a two-blade turbine is selected as a verification example, as shown in Fig. 1(a). The turbine has an overlap ratio of 0.1 and the experimental data can be found in Ref. [30]. Table 1 lists the geometrical parameters of the turbine. From the study of Ref. [5,7,30], it is known that the power coefficient of the vertical turbines is affected by their aspect ratios. Because the computational cost of a three-dimensional (3-D) unsteady simulation of a three-turbine cluster is much higher than that of a 2-D unsteady simulation, the common practice in optimizing turbine clusters is to conduct 2-D computations, as adopted in Ref. [24]. In the present study, the 2-D numerical model is adopted to facilitate optimizations.

Two parameters are used to verify the simulation model for the Savonius wind turbine, i.e., the moment coefficient C_m (as defined by Eq. (1)) and power coefficient C_P (as defined by Eq. (2)) against *TSR* (as shown in Eq. (3)) [31].

$$C_T = \frac{T}{0.5\rho \cdot U_{in}^2 \cdot A} \tag{1}$$

$$C_P = \frac{T \cdot \omega}{0.5\rho \cdot U_{in}^3 \cdot A} \tag{2}$$

$$TSR = \frac{\omega \cdot D}{2U_{in}} \tag{3}$$

where T, ω, U_{in}, D, and A are the torque, rotational speed, free-stream velocity of the wind, turbine diameter and turbine swept area, respectively.

The power coefficient ratio (f) is defined as Eq. (4) [32] to describe the enhancement of the turbine in a cluster.

$$f = C_P / C_{P,\ \text{isolated turbine}} \tag{4}$$

where C_P is the power coefficient of an individual turbine in a cluster and $C_{P,\ \text{isolated turbine}}$ is the power coefficient of the isolated turbine.

The computational domain is divided into four sub-domains, as shown in Fig. 1 (b). It includes the stationary Zone I (circling the turbines), Zone II (surrounding the wake region of turbines), Zone III (external region), and the rotational zones containing the turbines. The conformal conditions are employed for the interfaces between Zone I and II, as well as Zone II and III. For the interfaces between the rotational zones and Zone I, the sliding mesh models are adopted, as used in Ref. [33].

To prevent the blocking effect caused by the upper and lower boundary and allow the wakes of the wind turbines to develop sufficiently, the width of Zone III should be large [34]. For this purpose, the upstream semicircular boundary, the upper and lower boundary, which make up the inlet boundary, are all 15D away from the central rotor, while the outlet boundary is set to be 30D downstream away, which is similar to Ref. [22]. Zone II is scaled to 1/3 of Zone III, and the diameter of Zone I is set to be a value in a range of 3D to 4D depending on the position of the three rotors.

2.2. Grid generation and independence test

The distribution of a high-quality mesh around the turbines is shown in Fig. 2. The unstructured triangular grid is generated for the whole fluid domain except for the boundary layer near the turbine surfaces. Around the turbine surfaces, a structured quadrilateral grid of 16 layers is applied with a growth rate of 1.05, as shown in Fig. 2(b). The thickness of the first layer grid is set to be 0.05 mm, to ensure that the $y+$ is close to 1 and the flow separation phenomena can be captured [32]. Fig. 3 shows the $y+$ distribution around the turbine, and its maximum value is less than 1.5, which

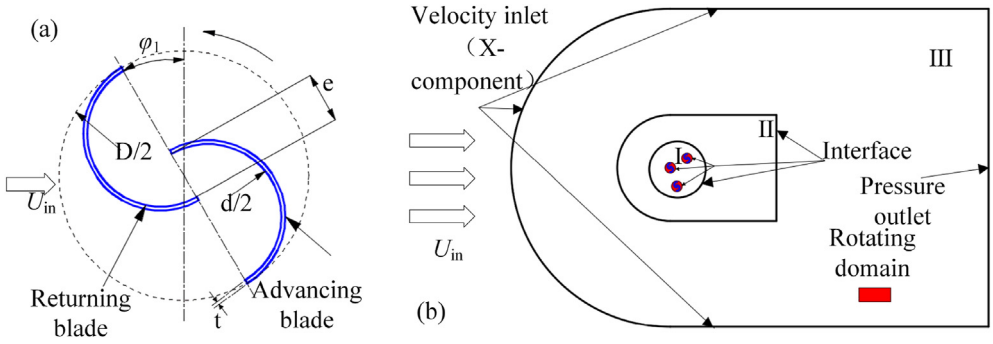

Fig. 1. The Sketch of the turbine (a) and computational domain (b).

Table 1
Geometrical parameters of the turbine.

Turbine geometry	Value
Number of blades	2
Blade diameter *d*	0.5 [m]
Turbine diameter *D*	0.95 [m]
Overlap ratio *s*	0.1
Overlap distance *e*	50 [mm]
Blade thickness *t*	1 [mm]
Turbine height *H*	1 [m]

meets the requirements of the *k*-*ω* SST turbulence model.

The verification results of grid independence for an isolated Savonius wind turbine are shown in Table 2. When the grid number is over 130,000, the change in C_P is around 1%. For fast simulations with reasonable accuracy, the grid with a number of 130 k is chosen for further simulations.

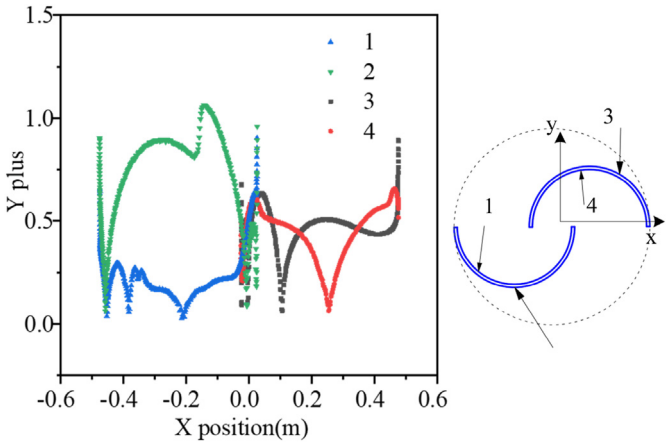

Fig. 3. The $y+$ value for the turbine at $\varphi = 90°$.

2.3. Computational models and numerical validation

Two-dimensional unsteady Reynolds-averaged Navier-Stokes *(RANS)* equations are solved by ANSYS FLUENT with *k*-*ω* SST turbulence model. This turbulence model is widely used in numerical simulations of Savonius turbines [24,26,35] because of its feasibility in high adverse pressure gradient and dynamic stall at low *TSR* conditions [36]. The X-velocity of 7 m/s is imposed at the inlet boundary and static pressure of 0 at the outlet boundary. Turbulence intensity and turbulent viscosity ratio are chosen to be 0.1% and 10, respectively, for the inlet and outlet boundary. No-slip wall condition is given on blade surfaces. In addition, other options are selected as pressure-based formulation, coupled algorithm, and second-order upwind scheme [37] in this calculation.

A comparison of C_P between numerical calculations and experimental data for an isolated turbine is shown in Fig. 4. It can be seen that when the tip speed ratio is less than 0.9, the numerical results fit the experimental data well. By contrast, the numerical results overestimate C_P to some extent, when the tip speed ratio is greater than 0.9, due to the 3-D effects [34]. The numerical optimal tip speed ratio (*TSR*) is 1.0 (14.737 rad/s) with a C_P of 0.245 for the

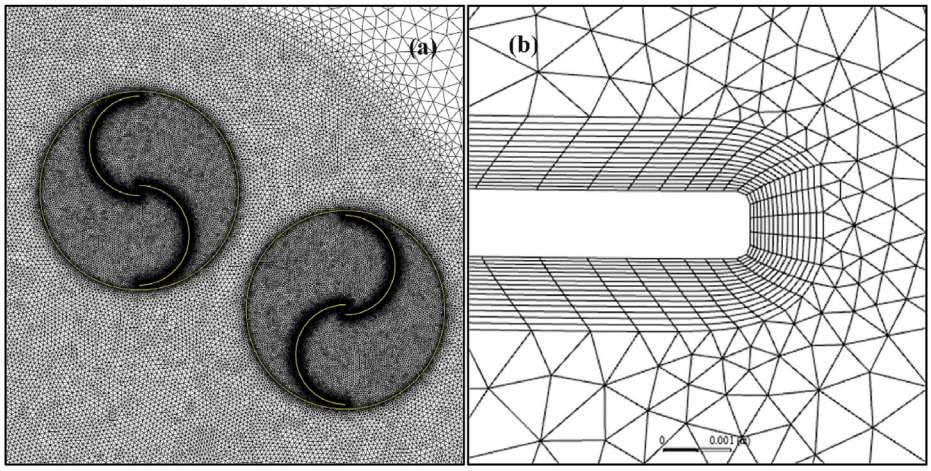

Fig. 2. Grid distribution around the turbines (a) and the boundary layers of the blade (b).

Table 2
Grid independence test.

Refinement level	Grid number	C_P	Error
1	52 k	0.2497	8.9%
2	81 k	0.2449	6.8%
3	130 k	0.2310	0.7%
4	208 k	0.2332	1.7%
5	301 k	0.2293	0

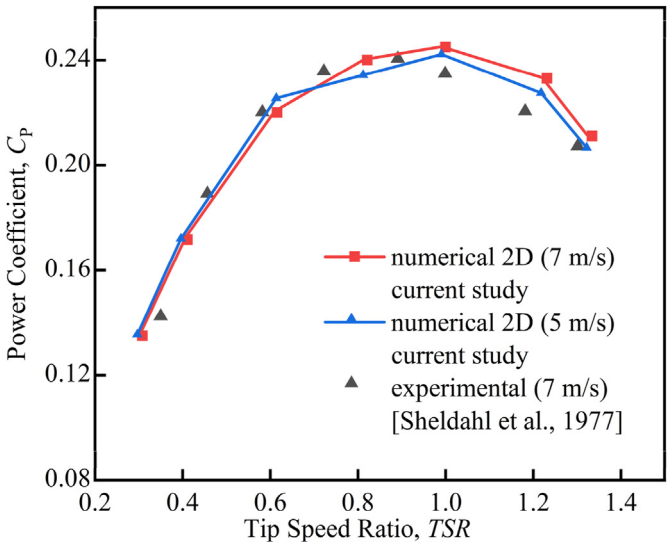

Fig. 4. The comparison of power coefficient between numerical results and the experimental data [30].

isolated wind turbine at a wind speed of 7 m/s. In addition, the numerical C_P curve at 5 m/s differs slightly from that at 7 m/s.

2.4. Time step independence

The time step for the unsteady simulations with a sliding interface should not be larger than the time it takes to move a cell characteristic size, as adopted in Ref. [32]. The time step is usually determined by making the rotor move at a specific angle (i.e. 0.5°, 1°) for a turbine with a constant speed. For the present proposed variable-speed turbine control cases, the rotational speed of each

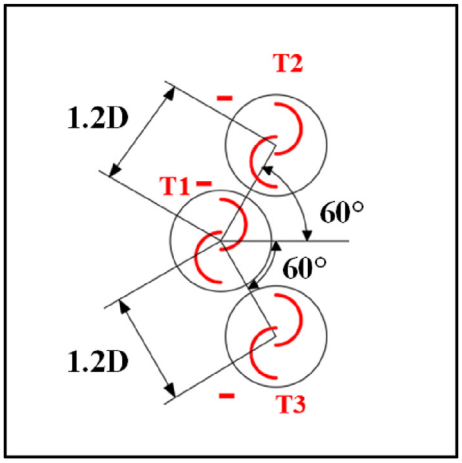

Fig. 5. The efficient cluster suggested by Ref. [22].

Table 3
Time step independence study.

Refinement level	Time step (s)	$\overline{C_P}$	Error
1	0.005	0.2589	23.9%
2	0.002	0.3177	6.6%
3	0.001	0.3372	0.9%
4	0.0005	0.3402	0

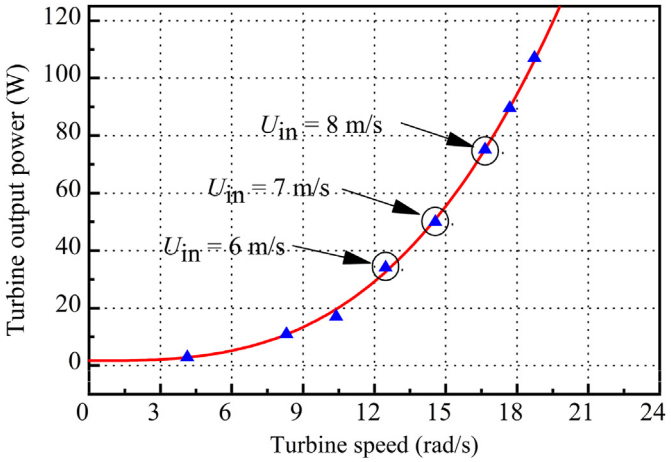

Fig. 6. The optimal power curve for the isolated turbine.

turbine is variable, so the time step independence is verified for the configuration shown in Fig. 5. Four time steps are tested in simulations, as listed in Table 3. Finally, the time step for level 3 is used in the following simulations.

2.5. The variable-speed control method

The strategy of the variable-speed control method is used to adjust the rotational speed of every turbine in a cluster, to make them operate on the optimal power curve of the isolated turbine. The optimal power curve can be obtained by two approaches: the first is to obtain the curve by modeling; the second is by simulation. Because the size of the Savonius turbine is not very large, the influence of the Reynolds number might not be neglected, as shown in Fig. 4. Therefore, the optimal power curve for the isolated turbine in this study is obtained by computing the power output at

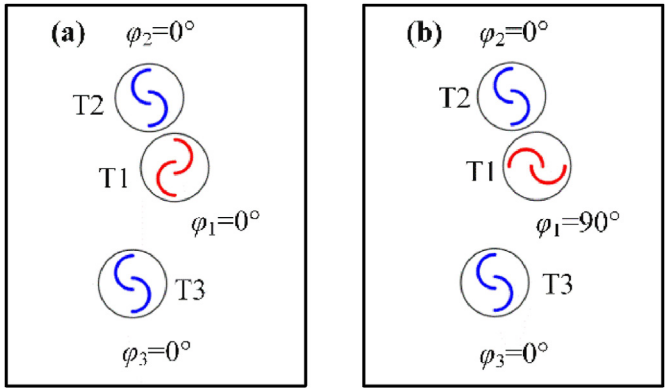

Fig. 7. The configuration of a designed cluster ($L_{1\text{-}2} = 1.2D$, $L_{1\text{-}3} = 2.0D$, $\theta_{1\text{-}2} = 110°$, $\theta_{1\text{-}3} = 110°$) of Case 1 (a) and Case 2 (b).

Table 4
The power coefficients of two cases.

	$C_{P,1}$	Rotational speed (rad/s)	$C_{P,2}$	Rotational speed (rad/s)	$C_{P,3}$	Rotational speed (rad/s)	$\overline{C_P}$
Case 1	0.359	17.86	0.324	16.37	0.307	15.88	0.33
Case 2	0.372	17.82	0.317	16.39	0.305	15.84	0.331

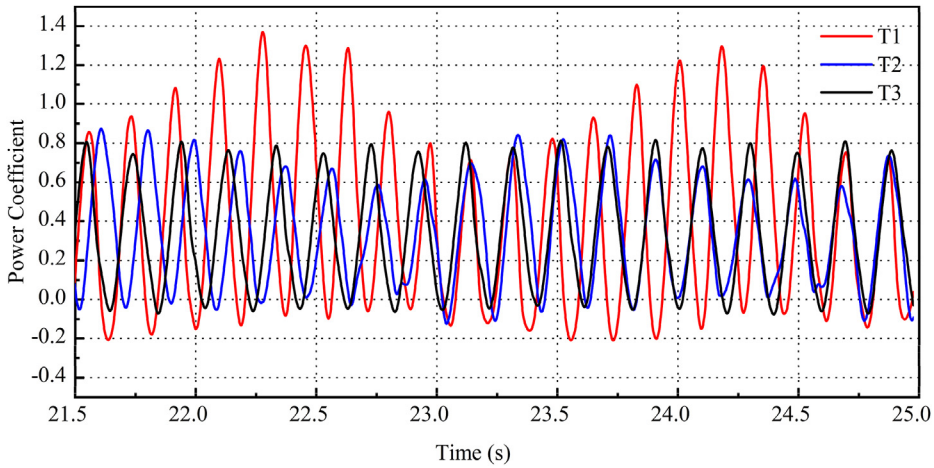

Fig. 8. Power coefficient time history of Case 1.

different *TSR* for every incoming flow velocity. The simulated optimal power output curve is shown in Fig. 6.

The power outputs of the turbines in a close cluster are different. This is because the incoming flow velocity for every turbine in a cluster is different due to the complex flows. If the power output of a turbine is above the optimal curve in Fig. 6, then the rotational speed of the turbine should be increased to match the point on the curve. The adjustment of the turbine speed is implemented by programming a User Defined Function code embedded in the Fluent software. In the present simulations, the speed adjustment process for the turbines in the cluster is considered to be completed when the changes in the rotational speed of the turbines are within 0.5 rad/s in the last 10 loops of speed adjustment. Actually, the final adjustment of the speed is within 0.1 rad/s in most cases.

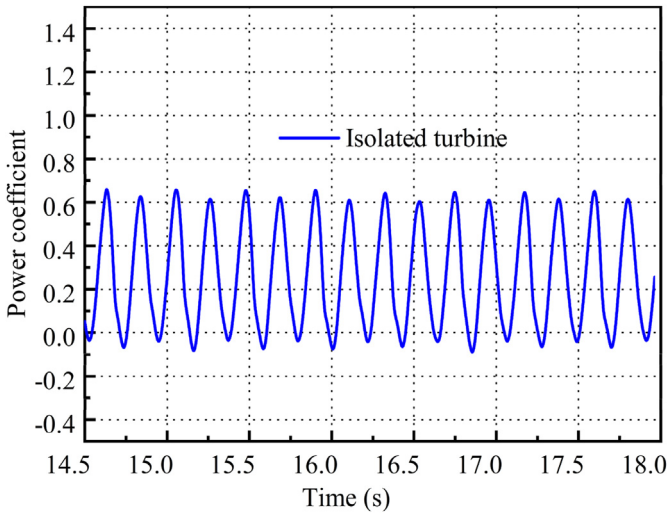

Fig. 9. Power coefficient time history of isolated turbine.

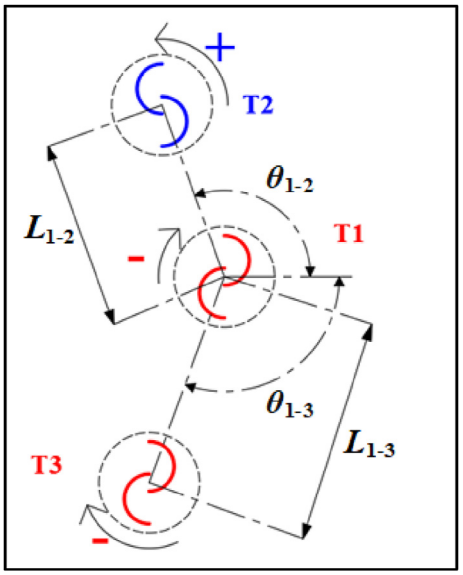

Fig. 10. Wind turbines configurations in a cluster.

Table 5
Factors and levels (Clockwise is -, anti-clockwise is +).

Levels / Factors	1	2	3	4
A ($L_{1\text{-}2}$)	1.2*D*	1.6*D*	2.0*D*	2.4*D*
B ($L_{1\text{-}3}$)	1.2*D*	1.6*D*	2.0*D*	2.4*D*
C ($\theta_{1\text{-}2}$)	30°	70°	110°	150°
D ($\theta_{1\text{-}2}$)	30°	70°	110°	150°
E (*RD*)	(-, -, -)	(-, -, +)	(-, +, +)	(-, +, -)

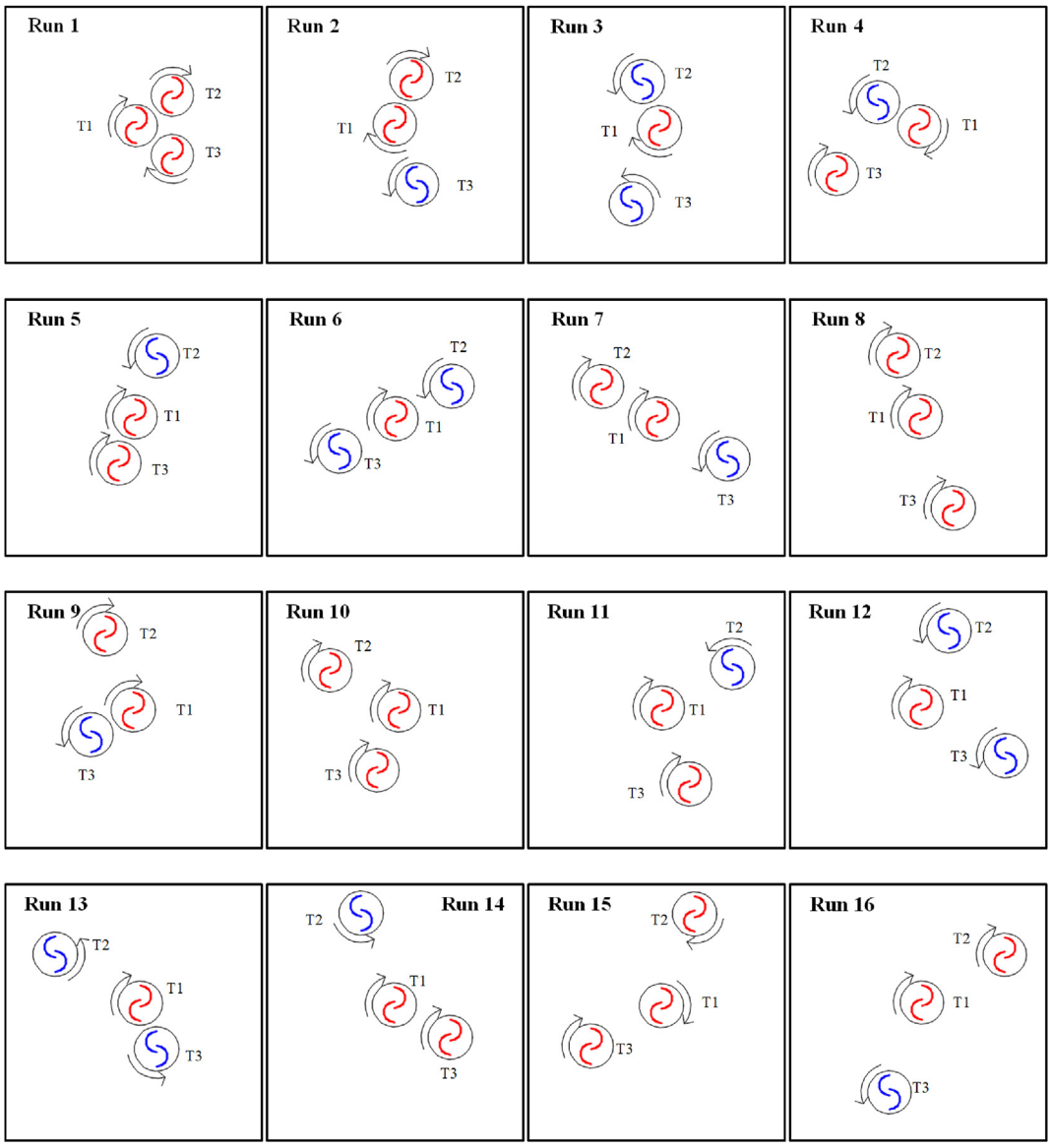

Fig. 11. The 16 designs of the Taguchi experiment.

Table 6
The power coefficients and S/N ratios of the 16 Runs.

No.	$L_{1\text{-}2}$ (m)	$L_{1\text{-}3}$ (m)	$\theta_{1\text{-}2}$ (°)	$\theta_{1\text{-}2}$ (°)	*RD*	$C_{P,\,1}$	$C_{P,\,2}$	$C_{P,\,3}$	$\overline{C_P}$	S/N
Run 1	1.2	1.2	40	40	(-, -, -)	0.1526	0.1778	0.1472	0.1592	−15.96
Run 2	1.2	1.6	70	70	(-, -, +)	0.2224	0.3043	0.3179	0.2815	−11.01
Run 3	1.2	2.0	110	110	(-, +, +)	0.3591	0.3241	0.3069	0.330	−9.63
Run 4	1.2	2.4	150	150	(-,+, -)	0.2706	0.3585	0.2670	0.2987	−10.50
Run 5	1.6	1.2	70	110	(-, +, -)	0.3487	0.3493	0.3034	0.3338	−9.53
Run 6	1.6	1.6	30	150	(-, +, +)	0.2642	0.2809	0.1874	0.2442	−12.25
Run 7	1.6	2.0	150	30	(-, -, +)	0.2446	0.2356	0.1969	0.2257	−12.93
Run 8	1.6	2.4	110	70	(-, -, -)	0.3374	0.3349	0.3099	0.3274	−9.70
Run 9	2.0	1.2	110	150	(-, -, +)	0.2596	0.3143	0.1838	0.2526	−11.95
Run 10	2.0	1.6	150	110	(-, -, -)	0.3241	0.3204	0.2655	0.3024	−10.39
Run 11	2.0	2.0	30	70	(-, +, -)	0.3522	0.320	0.3081	0.3268	−9.72
Run 12	2.0	2.4	70	30	(-, +, +)	0.2443	0.3129	0.2707	0.2759	−11.19
Run 13	2.4	1.2	150	70	(-, +, +)	0.2401	0.2586	0.2906	0.2631	−11.60
Run 14	2.4	1.6	110	30	(-, +, -)	0.3065	0.3170	0.2861	0.3032	−10.37
Run 15	2.4	2.0	70	150	(-, -, -)	0.2848	0.3729	0.2180	0.2919	−10.78
Run 16	2.4	2.4	30	110	(-, -, +)	0.2524	0.2780	0.2466	0.2590	−11.63

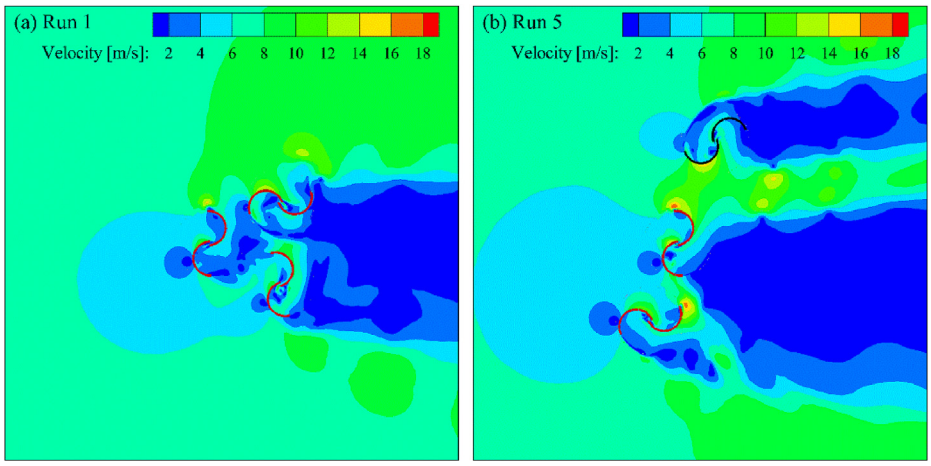

Fig. 12. Velocity contours around turbines in Run 1 (a) and Run 5 (b).

3. Results and discussion

3.1. Influence of the initial phase angle on the power of the turbine cluster

In previous investigations on a cluster of Savonius turbines, the initial phase angles for the turbines have been proved to be a crucial factor in power output, especially for the closely located turbines. The variable-speed control method is proposed to avoid the strict demand for accurate setting of the phase angle for the turbine. In this section, the influence of the initial phase angle on power output is analyzed for those turbines adopting the variable-speed control method. One configuration is designed as shown in Fig. 7. For this configuration, the relative phase angles of $\varphi_{1\text{-}2}$ and $\varphi_{1\text{-}3}$ both are 0° in Fig. 7(a) and are 90° in Fig. 6(b). The definition of $\varphi_{1\text{-}2}$ and $\varphi_{1\text{-}3}$ are given in the table of Nomenclature at the end of this paper. The simulated power coefficients (C_P) of the three turbines in Fig. 7(a) and (b), which are named Case 1 and 2, are listed in Table 4. The turbines rotating clockwise are marked red, while those rotating anti-clockwise are marked blue.

From Table 4, it can be seen that the average power coefficients ($\overline{C_P}$) of the two cases have nearly the same value and are both higher than that of the isolated turbine ($C_P = 0.245$), increasing by nearly 35%. In addition, the $\overline{C_P}$ of Case 1 differs from that of Case 2 to be less than 0.5%. The maximum difference of the C_P and rotational speed between the corresponding turbines in the two cases is less than 4%. By contrast, the phase angles of turbines at the same rotational speed in a cluster have a greater influence on the performance, resulting in a maximum difference of up to 50% in the power output of a three-turbine cluster [29]. It can be deduced that the simulation result of the proposed variable-speed control

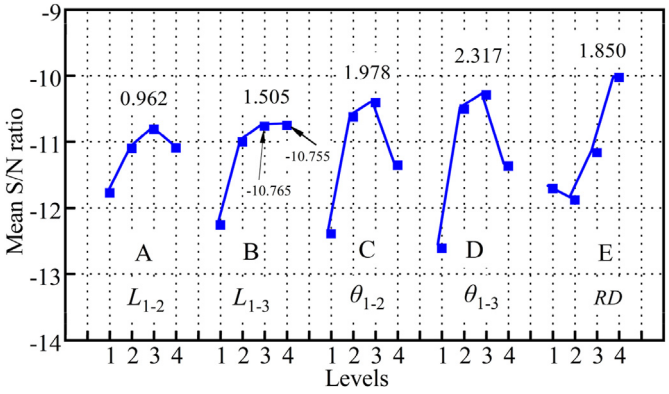

Fig. 14. The mean S/N ratio distributions of the five factors.

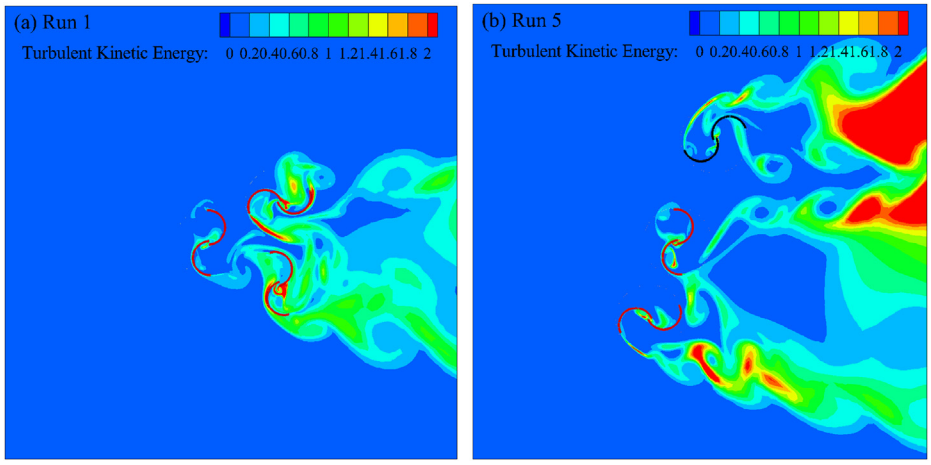

Fig. 13. Turbulence kinetic energy contours around turbines in Run 1 (a) and Run 5 (b).

method is not affected by the setting of the initial phase angles.

It is interesting to see the variations in the time series of the power coefficients of the turbines in the cluster. Because the fluctuation behaviors of C_P of the corresponding turbines in the two cases are similar, only the time series of C_P in Case 1 are shown in Fig. 8. For comparison, the time series of C_P of the isolated turbine is shown in Fig. 9. The amplitudes of the turbines in the cluster differ from each other considerably. The increase in the amplitude of T1 is noticeable. This may be because T1 is located closely to T2 and also in downstream of T2. By contrast, T3 has similar behavior to the isolated turbine, although its power output increases by nearly 25.3% due to the proximity to T1. This phenomenon can be explained by the fact that the influence of T1 is weakened due to the large distance (2*D*) between T1 and T3. In addition, in this condition, the power output of T3 is improved mainly from high-speed gap flow in the blocking region between turbines.

3.2. Optimization of Savonius wind turbine cluster

The Taguchi method is an efficient tool to rank the factors in a process and obtain the optimal factors and results [38]. It is also used in the optimization of the shapes of the VAWT [39,40] and the configuration of the VAWT cluster [41,42]. The Taguchi method is applied in this paper to optimize a wind turbine cluster composed of three wind turbines, with the rotational directions, separation distances, and angles of the configuration as factors, and the power output as the optimization objective.

3.2.1. Objective function

In this optimization, the corresponding loss function for the objective of large-the-better (LTB) is defined as follows [43]:

$$L_{\mathrm{LTB}} = \frac{1}{n}\sum_{1}^{n}\left[\left(\frac{1}{y_i}\right)^2\right] \tag{5}$$

where n is the number of repeated experiments, (n equals 1 in this work).

The signal-to-noise (S/N) ratio is calculated as a logarithmic transformation of L_{LTB}, as shown below:

$$S/N = -10\log\left[\left(\frac{1}{y_i}\right)^2\right] \tag{6}$$

where y_i represents the value of C_P in this study.

As it can be seen in Eq. (6), maximizing $\overline{C_P}$ can achieve the maximum value of the S/N ratio.

3.2.2. Factors and levels

The configuration of the three turbine clusters is shown in Fig. 10. T1 is placed at the origin of the coordinate system. Four factors are chosen to determine the configuration. They are the distance ($L_{1\text{-}2}$) between the centers of T1 and T2, the angle ($\theta_{1\text{-}2}$) between $L_{1\text{-}2}$ and the horizontal axis, the distance ($L_{1\text{-}3}$) between the centers of T1 and T3, and the angle ($\theta_{1\text{-}3}$) between $L_{1\text{-}3}$ and the horizontal axis. In addition, the combination of the rotational direction (*RD*) of the three turbines is also selected as a factor. The rotational speed and initial phase angle of each turbine are not considered as factors in the Taguchi method.

The levels of the five factors are listed in Table 5. The ranges of $L_{1\text{-}2}$ and $L_{1\text{-}3}$ are determined by referring to the results of Ref. [22]. The results of Ref. [22] showed that when $L_{1\text{-}2}$ and $L_{1\text{-}3}$ are both 1.2*D*, the power outputs of three turbines increased evidently; while the power outputs increase slightly when the distances are 2.4*D* apart. Therefore the range from 1.2*D* to 2.4*D* is selected for $L_{1\text{-}2}$ and $L_{1\text{-}3}$. In addition, the ranges of the angles of $\theta_{1\text{-}2}$ and $\theta_{1\text{-}3}$ are set from 30° to 150°, to avoid placing the turbine in the downstream region of another. The combination of rotational directions of the T2 and T3 has four conditions, with the fixed rotational direction of T1. Finally, an L_{16} (4^5) orthogonal array is chosen and the layouts of the 16 designs of the cluster are displayed in Fig. 11.

3.2.3. Analysis of Taguchi experiment

Table 6 lists the power coefficients ($C_{P,1}$, $C_{P,2}$, $C_{P,3}$) of the three turbines, the average power coefficient ($\overline{C_P}$) of the wind turbine cluster, and the S/N ratio for the CFD results of the 16 designs. It can be seen that Run 5 has the best $\overline{C_P}$ ($f = 1.36$), whereas the $\overline{C_P}$ of Run 1 is the lowest in all the 16 cases ($f = 0.65$). The $\overline{C_P}$ of Runs 1, 6, and 7 are lower than that of the isolated turbine but other $\overline{C_P}$ are not. In this round of design of experiment, the performance of the cluster is improved in most cases, due to the coupling effect.

Because the difference in power output between Run 1 and Run 5 is the largest in the 16 cases, it is necessary to make a comparison of the two velocity fields, which are shown in Fig. 12. The reason that the $\overline{C_P}$ of Run 1 is the lowest in all cases may be that the turbines T2 and T3 are in the wake of T1 (Fig. 12(a)), which results in a reduction of available wind energy to the downstream turbines, T2 and T3. Another important factor is rotational direction. In Fig. 12(b), it can be seen that T1 and T2 are counter-rotating. In addition, the high-speed gap flow between T1 and T2 is favorable to push the advancing blades to generate positive torque. The turbines in clusters of Runs 4, 11, and 14, which have the same rotational direction as Run 5, all generate more power than the isolated turbine. Fig. 13 shows the turbulence kinetic energy contours in the flow fields of Runs 1 and 5. Obviously, the turbulence kinetic energy

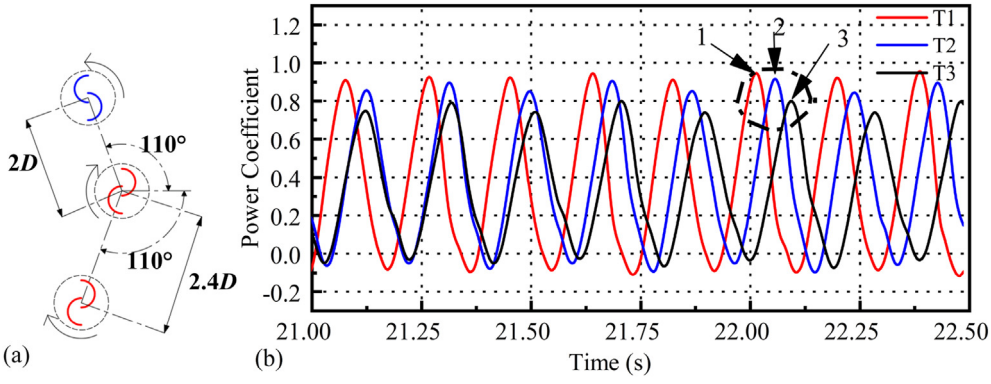

Fig. 15. The position of the three turbines in the optimal cluster (a) and the power coefficient of the three turbines (b).

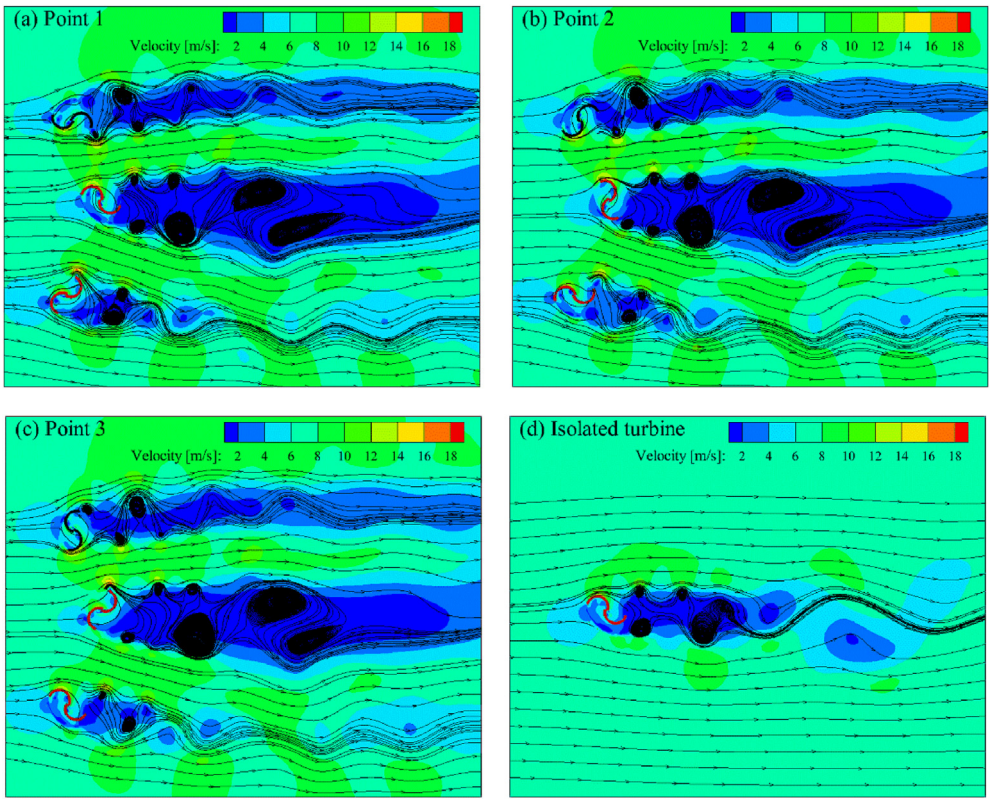

Fig. 16. The velocity contour of turbines in point 1 (a), point 2 (b), point3 (c), and the isolated turbine (d).

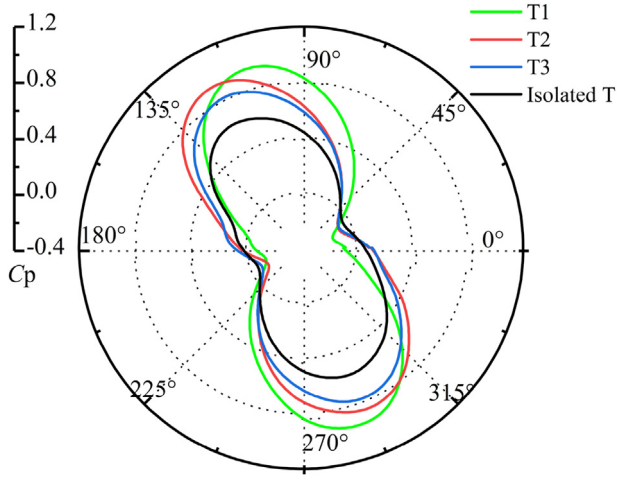

Fig. 17. The instantaneous value of power coefficient (C_P) versus azimuthal angle (0–360°) for three turbines in the optimal cluster and isolated turbine.

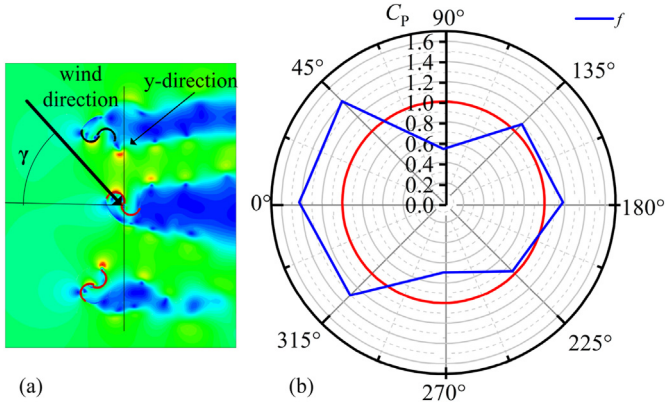

Fig. 18. The definition of wind direction (a) and the average power coefficient ratio versus wind direction (b).

around T2 and T3 in Run1 is much larger than that in Run5. This is also an indicator that T2 and T3 in Run 1 are much influenced by T1 and a fraction of the energy of the flow is wasted into turbulence kinetic energy.

From the above discussion, it is evident that the distances and angles between the turbines, which determine the configuration of the cluster, and the rotational direction all affect the power output of the individual turbine in the cluster, due to the interactions involving the gap flow in blocking region, wake flow, and favorable pushing force. It is necessary to evaluate the influence of the three parameters quantitatively, i.e. the distance, the angle, and the rotational direction, on the power output of the turbines because the unsteady flow is very complex.

For this purpose, the mean S/N ratio of the Taguchi method is used to make this evaluation. The mean S/N ratios of five factors are calculated by using the results in Table 6, and are shown in Fig. 14. The mean S/N ratio is calculated in the following way. For example, for Level 1 of Factor A ($L_{1\text{-}2}$), the mean S/N ratio is the average of the four S/N ratios of Factor A at Level 1. That is , S/N (A1) = (S/N (Run 1) + S/N (Run 2) + S/N (Run 3) + S/N (Run 4))/4 = −11.775. The range for every factor is labeled on the mean S/N ratio curves.

By carefully analyzing the results in Fig. 14, it can be observed: first, the shapes of the curve of the mean S/N ratios for Factor A and B are not similar, because the rotational direction of T1 is fixed in the present investigations. From Fig. 11 it can be seen that the

advancing blade of T1 is always on the side of T2 while the returning blade is always on the side of T3. This makes the flow field unsymmetrical. Second, the mean S/N values of Factor C and D at their Level 1 and 4 are very low. This is because Level 1 of Factor C and D corresponds to the configurations in which T2 and T3 are in the downstream region of T1, while Level 4 of Factor C and D represent that T1 is in the downstream region of T2 and T3. This will reduce the power output of the cluster with an underlying mechanism similar to Run 1. Third, the ranges labeled on the curves in Fig. 14 represent the influence of factors on the power output of the wind turbine cluster. The influence order of the five factors is $\theta_{1\text{-}3} > \theta_{1\text{-}2} > RD > L_{1\text{-}3} > L_{1\text{-}2}$, which means the influence of the configuration angle weighs heavier than that of the combination of rotational direction, and the distance is the least important parameter.

3.2.4. The power output of the optimal cluster

The three-turbine cluster will have the maximum power output when the five factors are at the levels with the maximum value of mean S/N ratios, as used in Ref. [41]. Therefore, the optimal level combination of the five factors is $L_{1\text{-}2} = 2.0D$, $L_{1\text{-}3} = 2.4D$, $\theta_{1\text{-}2} = 110°$, $\theta_{1\text{-}3} = 110°$ and $RD = (-, +, -)$, as shown in Fig. 15(a). The $C_{P,1}$, $C_{P,2}$ and $C_{P,3}$ are 0.357, 0.365, and 0.325 when the *TSR*s of the T1, T2, and T3 are 1.13, 1.14, and 1.09, respectively; and $\overline{C_P}$ for the cluster is 0.349 ($f = 1.425$). The time series of C_P of the three turbines are shown in Fig. 15(b). It is worth noticing that the peak value fluctuation of C_P of T1 almost disappears due to a large distance between T1 and T2.

3.3. Analysis of the flow fields of the optimal cluster

The flow fields of the optimal cluster at three instants are shown in Fig. 16(a), (b), and (c). The three instants correspond to the times when the power coefficients of the three turbines reach their peaks, as labeled by Points 1, 2, and 3 in Fig. 15(b). The power coefficients of the three turbines rank as T2 > T1 > T3, and the underlying mechanism, similar to Run 5, has been explored. Indeed, the high-speed gap flow in the blocking region between T1 and T2 pushes their advancing blades to increase the torques of both T1 and T2. In the meantime, the gulped incoming flow between T2 and T3 will also increase the flow speed between T1 and T3. On the one hand, this increased gap flow is beneficial to the torque generation of T3; on the other hand, it will reduce the power output of T1 to some extent. However, the gap flow between T1 and T2 is higher than that between T1 and T3, as can be seen in Fig. 16. The net effect for T1 is the rise of its torque. In addition, from the velocity fields, it can be seen that the wake region of T1 is the largest, while that of T3 is the smallest. The reason is supposed to be that more power is extracted from the fluid by T1 than by T3. Similarly, the wake of T2 is larger than that of T3, because $C_{P,2}$ is larger than $C_{P,3}$, although T2 has a favorable fluid field to generate a high torque. Furthermore, the fluctuation magnitude of $C_{P,1}$ is the largest, while that of $C_{P,3}$ is the lowest, as shown in Fig. 15(b). From Fig. 16, it is clearly seen that there are two high-speed gap flows surrounding T1 and they oscillate due to the rotational of the blade, which is responsible for the large fluctuation of $C_{P,1}$.

The polar chart of the power coefficients versus phase angle of the three turbines in the optimal cluster and the isolated turbine is shown in Fig. 17. The definition of the phase angle is shown in Fig. 1(a) and the scale of C_P in Fig. 17 is displayed on the right-hand side to make it easy to identify. Although the shapes of the polar charts of C_P of the turbines in the cluster look similar to that of the isolated turbine, the amplitudes are larger and there are some distortions in the power coefficients due to the interactions between turbines. This implies that the essential flow feature of the Savonius turbine remains, but the transient flow field around every turbine in the cluster is different from each other and from the isolated turbine, due to the coupling effect.

The overall power output of the wind turbine cluster would be affected by wind flow direction. For the present optimal cluster configuration, the power coefficients were investigated in eight wind directions to study the influence of flow directions. Fig. 18 shows the average power coefficient ratio (f) of the optimal turbine cluster versus wind direction (γ). It can be seen that there is a range from −45° to 45° where the $\overline{C_P}$ of this cluster is improved by at least 30% more than that of the isolated turbine. The performance of the cluster will deteriorate if the wind is in the y-direction. Therefore, the optimal configuration of the present wind cluster is more suitable for situations with prevailing wind directions.

4. Conclusion and future work

The present variable-speed control method provides an easy strategy to improve the power output of a cluster of turbines. The power output of a cluster of three variable-speed turbines is optimized by using the Taguchi method. The optimal configuration and rotational speeds of the three-turbine cluster are determined, and the corresponding flow fields are studied in detail. Some conclusions are summarized below:

(1) The proposed variable-speed control method to improve the power output of the cluster of the turbines is not affected by the initial phase angles of the turbines, despite the fact that the initial phase angle is a crucial factor to influence the power output of the cluster of turbines operating at the same rotational speed.
(2) The $\overline{C_P}$ of the optimal cluster is 0.349, which is increased by 42.5% than that of the isolated turbine. In addition, the tip speed ratios for the three turbines are 1.13, 1.14, and 1.09, which are different from each other due to the locally different incoming flow fields.
(3) The influence strength order is ranked as the angle factor, rotational direction factor, length factor. In addition, two important combinations of the influential factors were identified: the worst combination of the angle factors in which one turbine is located in the wake of another turbine; and the best combination of rotational directions in which the advancing blades of three turbines are located in the blocking region between adjacent turbines.

In future work, the improvement effect of the modified shape and the aspect ratio of the Savonius turbine on the power output of the turbines in the optimal configuration is worthy of further investigation.

CRediT authorship contribution statement

Yunrui Chen: Conceptualization, Methodology, Software, Writing – original draft. **Penghua Guo:** Conceptualization, Resources, Supervision. **Dayu Zhang:** Methodology, Validation. **Kaixin Chai:** Software. **Chenxi Zhao:** Visualization. **Jingyin Li:** Writing – review & editing, Funding acquisition.

Declaration of competing interest

The authors declare that they have no known competing financial interests or personal relationships that could have appeared to influence the work reported in this paper.

Acknowledgments

The authors gratefully acknowledge the financial support provided by the National Natural Science Foundation of China (51876158) and the National Major Science and Technology Projects of China (2017-II-0007-0021).

Nomenclature

d	Bucket diameter [m]
D	Turbine diameter [m]
H	Turbine height [m]
e	Distance of overlap [mm]
t	Turbine thickness [mm]
s	Overlap ratio (e/d)
T1	Turbine 1 in a cluster (similar T2 and T3)
φ_1	Angle between the flow and the line joining centers the two buckets (similar φ_2 and φ_3)
$\varphi_{1\text{-}2}$	Realtive phase angle between T1 and T2 ($\varphi_{1\text{-}2} = \varphi_1 - \varphi_2$)
$\varphi_{1\text{-}3}$	Realtive phase angle between T1 and T3 ($\varphi_{1\text{-}3} = \varphi_1 - \varphi_3$)
$\theta_{1\text{-}2}$	Angle between the line joining centers between T1 and T2 and the incoming flow
$\theta_{1\text{-}3}$	Angle between the line joining centers between T1 and T3 and the incoming flow
$L_{1\text{-}2}$	Distance of the centers between T1 and T2
$L_{1\text{-}3}$	Distance of the centers between T1 and T3
RD	Rotational direction of three turbines
C_m	Average power coefficient of turbine
C_P	Power coefficient of a turbine
$C_{P,\,1}$	Power coefficient of T1 (similar $C_{P,\,2}$ and $C_{P,\,3}$)
$\overline{C_P}$	Average power coefficient of a cluster
γ	Angle of wind direction

References

[1] T. Zhou, D. Rempfer, Numerical study of detailed flow field and performance of Savonius wind turbines, Renew. Energy 51 (2013) 373–381.
[2] I. Ostos, I. Ruiz, M. Gajic, W. Gómez, A. Bonilla, C. Collazos, A modified novel blade configuration proposal for a more efficient VAWT using CFD tools, Energy Convers. Manag. 180 (2019) 733–746.
[3] I. Marinić-Kragić, D. Vučina, Z. Milas, Computational analysis of Savonius wind turbine modifications including novel scooplet-based design attained via smart numerical optimization, J. Clean. Prod. 262 (2020), 121310.
[4] N.H. Mahmoud, A.A. El-Haroun, E. Wahba, M.H. Nasef, An experimental study on improvement of Savonius rotor performance, Alex. Eng. J. 51 (2012) 19–25.
[5] I. Marinić-Kragić, D. Vučina, Z. Milas, Global optimization of Savonius-type vertical axis wind turbine with multiple circular-arc blades using validated 3D CFD model, Energy 241 (2022), 122841.
[6] J.V. Akwa, G. Alves da Silva Júnior, A.P. Petry, Discussion on the verification of the overlap ratio influence on performance coefficients of a Savonius wind rotor using computational fluid dynamics, Renew. Energy 38 (2012) 141–149.
[7] K. Sobczak, Numerical investigations of an influence of the aspect ratio on the Savonius rotor performance, J. Phys. Conf. Ser. 1101 (2018), 012034.
[8] A.S. Saad, I.I. El-Sharkawy, S. Ookawara, M. Ahmed, Performance enhancement of twisted-bladed Savonius vertical axis wind turbines, Energy Convers. Manag. 209 (2020), 112673.
[9] M.M. Kamal, R.P. Saini, A numerical investigation on the influence of savonius blade helicity on the performance characteristics of hybrid cross-flow hydrokinetic turbine, Renew. Energy 190 (2022) 788–804.
[10] T. Micha Premkumar, S. Sivamani, E. Kirthees, V. Hariram, T. Mohan, Data set on the experimental investigations of a helical Savonius style VAWT with and without end plates, Data Brief 19 (2018) 1925–1932.
[11] A.S. Saad, A. Elwardany, I.I. El-Sharkawy, S. Ookawara, M. Ahmed, Performance evaluation of a novel vertical axis wind turbine using twisted blades in multi-stage Savonius rotors, Energy Convers. Manag. 235 (2021), 114013.
[12] K.C. Sarma, A. Biswas, R.D. Misra, Experimental investigation of a two-bladed double stage Savonius-akin hydrokinetic turbine at low flow velocity conditions, Renew. Energy 187 (2022) 958–973.
[13] K. Golecha, T.I. Eldho, S.V. Prabhu, Influence of the deflector plate on the performance of modified Savonius water turbine, Appl. Energy 88 (2011) 3207–3217.
[14] S.A. Payambarpour, A.F. Najafi, F. Magagnato, Investigation of deflector geometry and turbine aspect ratio effect on 3D modified in-pipe hydro Savonius turbine: parametric study, Renew. Energy 148 (2020) 44–59.
[15] A. Pallotta, D. Pietrogiacomi, G.P. Romano, HYBRI – a combined Savonius-Darrieus wind turbine: performances and flow fields, Energy 191 (2020), 116433.
[16] R. Mereu, D. Federici, G. Ferrari, P. Schito, F. Inzoli, Parametric numerical study of Savonius wind turbine interaction in a linear array, Renew. Energy 113 (2017) 1320–1332.
[17] T. Ogawa, Study of a Savonius-type wind turbine: 4th report. Effects of the mutual interaction, Trans. Jpn. Soc. Mech. Eng. Ser. B. 52 (1986) 3259–3265.
[18] K. Golecha, T.I. Eldho, S.V. Prabhu, Study on the interaction between two hydrokinetic savonius turbines, Int. J. Rotating Mach. (2012) (2012) 1–10.
[19] C.M. Jang, Y.G. Kim, S.K. Kang, J.H. Lee, An experiment for the effects of the distance and rotational direction of two neighboring vertical Savonius blades: effects of distance and rotational direction of VAWT blades, Int. J. Energy Res. 40 (2016) 632–638.
[20] A. Shigetomi, Y. Murai, Y. Tasaka, Y. Takeda, Interactive flow field around two Savonius turbines, Renew. Energy 36 (2011) 536–545.
[21] A.K. Nag, S. Sarkar, Performance analysis of Helical Savonius Hydrokinetic turbines arranged in array, Ocean Eng. 241 (2021), 110020.
[22] M. Shaheen, M. El-Sayed, S. Abdallah, Numerical study of two-bucket Savonius wind turbine cluster, J. Wind Eng. Ind. Aerod. 137 (2015) 78–89.
[23] M. Shaheen, S. Abdallah, Development of efficient vertical axis wind turbine clustered farms, Renew. Sustain. Energy Rev. 63 (2016) 237–244.
[24] Y. Zheng, H.L. Bai, C.M. Chan, Optimization of Savonius turbine clusters using an evolutionary based Genetic Algorithm, Energy Proc. 158 (2019) 637–642.
[25] A.R. El-Baz, K. Youssef, M.H. Mohamed, Innovative improvement of a drag wind turbine performance, Renew. Energy 86 (2016) 89–98.
[26] M.A.A. Meziane, E. Essadiqi, M. Faqir, M.F. Ghanameh, CFD study of unsteady flow through savonius wind turbine clusters, Int. J. Renew. Energy Resour. 9 (2019) 657–666.
[27] B. Belabes, A. Youcefi, M. Paraschivoiu, Numerical investigation of Savonius wind turbine farms, J. Renew. Sustain. Energy 8 (2016), 053302.
[28] R.V. Bethi, S. Mitra, P. Kumar, An OpenFOAM based study of Savonius turbine arrays in tunnels for power maximisation, Renew. Energy 179 (2021) 1345–1359.
[29] X.J. Sun, D.H. Luo, D.G. Huang, G.Q. Wu, Numerical study on coupling effects among multiple Savonius turbines, J. Renew. Sustain. Energy 4 (2012), 053107.
[30] R.E. Sheldahl, B.F. Blackwell, L.V. Feltz, Wind tunnel performance data for two- and three-bucket Savonius rotors, J. Energy 2 (1978) 160–164.
[31] A. Grönman, J. Tiainen, A. Jaatinen-Värri, Experimental and analytical analysis of vaned savonius turbine performance under different operating conditions, Appl. Energy 250 (2019) 864–872.
[32] S. Zanforlin, Advantages of vertical axis tidal turbines set in close proximity: a comparative CFD investigation in the English Channel, Ocean Eng. 156 (2018) 358–372.
[33] J.W. Zhong, J.Y. Li, P.H. Guo, Y. Wang, Dynamic stall control on a vertical axis wind turbine aerofoil using leading-edge rod, Energy 174 (2019) 246–260.
[34] G. Ferrari, D. Federici, P. Schito, F. Inzoli, R. Mereu, CFD study of Savonius wind turbine: 3D model validation and parametric analysis, Renew. Energy 105 (2017) 722–734.
[35] L.B. Kothe, S.V. Möller, A.P. Petry, Numerical and experimental study of a helical Savonius wind turbine and a comparison with a two-stage Savonius turbine, Renew. Energy 148 (2020) 627–638.
[36] R. Nobile, M. Vahdati, J.F. Barlow, A. Mewburn-Crook, Unsteady flow simulation of a vertical axis augmented wind turbine: a two-dimensional study, J. Wind Eng. Ind. Aerod. 125 (2014) 168–179.
[37] F. Balduzzi, A. Bianchini, R. Maleci, G. Ferrara, L. Ferrari, Critical issues in the CFD simulation of Darrieus wind turbines, Renew. Energy 85 (2016) 419–435.
[38] M. Altan, Reducing shrinkage in injection moldings via the Taguchi, ANOVA and neural network methods, Mater. Des. 31 (2010) 599–604.
[39] Z.Y. Wang, Y.C. Wang, M. Zhuang, Improvement of the aerodynamic performance of vertical axis wind turbines with leading-edge serrations and helical blades using CFD and Taguchi method, Energy Convers. Manag. 177 (2018) 107–121.
[40] M.H. Khanjanpour, A.A. Javadi, Optimization of the hydrodynamic performance of a vertical Axis tidal (VAT) turbine using CFD-Taguchi approach, Energy Convers. Manag. 222 (2020), 113235.
[41] W.H. Chen, C.Y. Chen, C.Y. Huang, C.J. Hwang, Power output analysis and optimization of two straight-bladed vertical-axis wind turbines, Appl. Energy 185 (2017) 223–232.
[42] M. Hassanpour, L.N. Azadani, Aerodynamic optimization of the configuration of a pair of vertical axis wind turbines, Energy Convers. Manag. 238 (2021), 114069.
[43] L.K. Sharma, S. Sharma, Y. Dubey, L. Parwani, Taguchi Method Approach for Multi Factor Optimization of S1 Tool Steel in Electrochemical Machining, 6, 2019, p. 8.